1. Structure of Surfaces

1.1. Basic Concepts of Surface Crystallography

Near surfaces, material properties differ from the bulk in several mono-layers below the surface. The surface unit cell of periodicity therefore contains necessarily more atoms than the bulk unit cell structure. Frequently, the surface unit cell is also in the plane parallel to the surface substantially larger than the bulk unit cell. For example the Si (111) surface unit cell contains 49 atoms in one layer and differs for about 4 layers from the bulk structure.

Instead of a three dimensional lattice composed of the vectors

$$\vec{R} = n_1 \vec{a}_1 + n_2 \vec{a}_2 + n_3 \vec{a}_3 \qquad n_1 n_2 n_3 \in \mathbb{Z}$$

we characterize the surface lattice by the translation vectors

$$\vec{S} = m_1 \vec{b}_1 + m_2 \vec{b}_2$$

The parallelogram spanned by the two vectors $\vec{b}_1$ and $\vec{b}_2$ is a primitive (minimum size) unit cell. As for a bulk lattice, the surface looks identical if viewed from any of the lattice points defined by the translations.

Similar to the bulk case, the crystal structure is composed of a lattice and a basis. Note that the basis is usually not composed only of atoms found in a plane but of all atoms with lateral coordinates within a given primitive cell and in the few topmost layers, where atoms have different positions compared to the bulk.

Similar to the 3D bulk Wigner-Seitz primitive cell, we may construct a 2D surface Wigner-Seitz cell.

While for the 3D bulk 14 Bravais-lattices exist, this number is reduced to 5 Bravais-lattices in 2D which are displayed in Fig. 1.1

Taking into consideration that the basis attached to a lattice point may reduce the symmetry, we arrive at only 17 crystallographic space groups in 2D (compared to 230 in 3D).

The positions of atoms at a surface differ from the bulk ones due to broken symmetry and broken bonds, which give rise to atomic rearrangements If the surface unit cell and its basis remain identical to the one of the truncated bulk, the changes near a surface consist only in a variation of interlayer spacing or a parallel shift of surface atoms and are named relaxation. If the surface unit cell or the arrangement of the atoms in the basis (for the materials own atoms) is changed, we talk of a reconstruction. (compare Fig.1.2)
If the crystal structure of the 2D lattice at the surface has a larger unit mesh we talk of a superstructure or superlattice. A superstructure may result from an adsorbed phase or a reconstruction. Note also that adsorption may induce a reconstruction.
Park and Madden introduced a matrix notation to relate the primitive superstructure translations $\vec{b}_1$ and $\vec{b}_2$ to those of the truncated bulk $\vec{a}_1$ and $\vec{a}_2$:

$$\vec{b}_1 = U_{11}\,\vec{a}_1 + U_{12}\,\vec{a}_2$$
$$\vec{b}_2 = U_{21}\,\vec{a}_1 + U_{22}\,a_2$$

The matrix $U = \begin{pmatrix} U_{11} & U_{12} \\ U_{21} & U_{22} \end{pmatrix}$ unambigeously specifies the larger super-structure unit mesh. If the $U_{ij} \in \mathbb{Z}$, all positions $m_1\vec{b}_1 + m_2\vec{b}_2$ are identical with respect to the substrate. If the U_{ij} are rational the superstructure is called commensurable, if they are irrational numbers it is called incommensurable. The distinction is partly academic as there are no experimental tools to rule out a rational relationship

between the substrate and the superstructure. Talking about an in-commensurate superstructure means that the lattice of the adsorbates does not lock into the underlying substrate lattice (this takes place e.g. if there is only little interaction between the two).

Although the matrix notation is exact and unambiguous, usually a more simple and intuitive notation introduced by Wood is used. For truncated bulk surface unit vectors $\vec{a}_1, \vec{a}_2$ and superstructure unit vectors $\vec{b}_1, \vec{b}_2$ we write

$$X(hkl) \; P/_C \left(\frac{|\vec{b}_1|}{|\vec{a}_1|} \times \frac{|\vec{b}_2|}{|\vec{a}_2|} \right) - R\varphi^° - n\cdot Ads$$

were :

$X(hkl) \triangleq$ material and Miller-index of plane

$P/_C \triangleq$ for primitive or centered unit cell; p is often omitted

$R\varphi^° \triangleq$ indicates the rotation angle φ between the two meshes; omitted for $\varphi = 0°$

vi. Ads $\triangleq$ in case of an adsorbate induced super-structure the type of adsorbate is specified and its number per unit cell n is specified

Examples : Si (111) (7×7)
Si (100) $c(4 \times 2)$
Si (111) $(\sqrt{3} \times \sqrt{3}) - R\,30° - 3\,Bi$

A few examples are shown in Fig. 1.3

Finally, the lattice reciprocal to the 2D lattice of the surface

unit vectors $\vec{a}_1, \vec{a}_2$ of the truncated bulk is given by

$$\vec{G}_{hk} = h \, \vec{a}_1^* + k \, \vec{a}_2^* \qquad\qquad h, k \in \mathbb{Z}$$

and $\qquad \vec{a}_i \cdot \vec{a}_j^* = 2\pi \delta_{ij}$

Explicitly, we may calculate

$$\vec{a}_1^* = 2\pi \, \frac{\vec{a}_2 \times \vec{n}}{|\vec{a}_1 \times \vec{a}_2|} \qquad \text{and} \qquad \vec{a}_2^* = 2\pi \, \frac{\vec{n} \times \vec{a}_1}{|\vec{a}_1 \times \vec{a}_2|}$$

where $\vec{n}$ is a unit vector normal to the surface.

The reciprocal vectors for a 2D lattice are normal to the corresponding real space vectors in the same plane as $\vec{a}_1$ and $\vec{a}_2$. Their absolute values are

$$|\vec{a}_1^*| = \frac{2\pi}{|\vec{a}_1| \cdot \sin(\measuredangle(\vec{a}_1, \vec{a}_2))} \qquad \text{and similar for } \vec{a}_2.$$

Fig. 1.4 displays a number of examples for unit meshes in real and reciprocal space. For a given 2D - Bravais lattice, the reciprocal one is of the same type.

Evidently, we may also define for super structure primitive translations $\vec{b}_1, \vec{b}_2$ the corresponding reciprocal vectors $\vec{b}_1^*, \vec{b}_2^*$.

When investigating the electronic structure of surfaces it is often useful to link the surface Brillouin zones to the 3D bulk Brillouin zones of the underlying 3D lattice. Two examples are shown in Fig. 1.5

1.2 Examples for surface structures

In this sub chapter we will consider just a few examples for metal and semiconducter surface structures

Surfaces of fcc crystals

Many metals crystallize in fcc structure, e.g. Cu, Ag, Au, Ni, Rh, Pd, Ir, Pt Fig. 1.6 displays the unreconstructed fcc {111}, {100} and {110} surfaces as they are found for Ni, Cu, Rh, Pd and Ag.
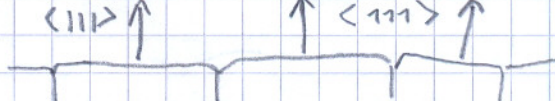
The coordination numbers of the surface atoms are 9, 8, 7, the numbers of broken bonds thus 3, 4, 5 for the {111} {100} and {110} surfaces

For the open {110} surface not only the uppermost atoms have broken bonds but also the second layer atoms have 1 broken bond per unit cell, resulting in total to 6 broken bonds per surface unit cell. In a simple nearest neighbour model each bond costs an energy $\frac{1}{12} E_c$ (E_c = cohesive energy) and the surface energies per unit cell are thus $\frac{1}{4} E_c$, $\frac{1}{3} E_c$ and $\frac{1}{2} E_c$. In order to obtain the specific surface energies γ, i.e. the surface energies per unit area, we have to take into account the different sizes of the unit cells. In units of $\frac{E_c}{a^2}$, with $a =$ lattice constant

we obtain $\gamma_{111} = 0,577$, $\gamma_{100} = 0,666$ and $\gamma_{110} = 0,707$. In reality the differences in γ are smaller, as the bond strength is not constant but monotonically decreasing with the number of bonds already existing [It is difficult to break a dimer bond compared to reduce the coordination from 12 to 11 (see Fig. 1.7)]. The fact that the {111} surface has the lowest surface energy is the deeper reason, why in polycrystalline films of fcc metals usually a {111} texture is found

As mentioned above, generally the bond strength depends on the coordination: The lower the coordination, the more the electrons will be redistributed to strengthen the remaining bonds, implying

a shorter bond length. In chemistry this argument is called bond order-
- bond length argument. Accepting this we expect for surface atoms
  - a decrease of the spacing between the two topmost layers, i.e. a
    negative value of $\Delta d_{12} = \dfrac{d_{12} - d_{bulk}}{d_{bulk}}$

  - a significant amount of tensile stress within the topmost
    layer

While Δd_{12} remains almost unchanged for $\{111\}$ and $\{100\}$ faces,
a significant relaxation with a change of Δd_{12} in the expected direction
is observed for $\{110\}$ surfaces. The Δd_{12} values for a number of
metals are tabulated in Fig 1.8.

However, for a number of $\{111\}$ and $\{100\}$ faces the tensile stress
becomes so large that the atoms leave the registry of the underlying
substrate and form a reconstruction. These reconstruction involve a
significant increase of the surface atomic density by up to 20%,
accompanied by a corresponding decrease of bond length and thus
of tensile stress. Consequently the surface energy of the reconstructed
surface is lowered.

The $\{100\}$ surfaces of Au, Pt, Ir all form a quasi-hexagonal surface
layer. Fig. 1.9 displays a structure model and an STM topograph of the
quasi-hexagonal reconstruction of Pt(001).

The $\{111\}$ surface of Au (and at high T also the one of Pt) forms a
1×22 reconstruction, involving an uniaxial compression of 4,5%.
The reconstruction involves the formation of two Shockley partial
dislocations, such that the topmost layer is partly in fcc and partly in
hcp stacking with compressed areas in between. From large scale
STM topographs it is apparent, that part of the elastic energy is released
by forming a higher order reconstruction - the socalled „herringbone"

reconstruction (Fig. 1.10)

Finally, we note that the $\{110\}$ faces of Au, Pt and Ir form missing row reconstructions. This reconstruction may be understood again as an energy minimizing process, by considering that the reconstructed surface consists of small $\{111\}$ facets, which are the ones of lowest energy (Fig. 1.11)

Surfaces of bcc crystals

The surfaces of bcc crystals have a prominent history in surface science due to the intense research on W in relation to its use as electron emitter. Though the symmetry of the low index surfaces $\{111\}, \{100\}, \{110\}$ is identical to the corresponding ones of fcc surfaces, the packing density and thus the order of specific surface energies γ is reversed. Most densely packed is the $\{110\}$ face forming a distorted hexagonal layer with a packing density of about 92% of hexagonal close packing. The $\{111\}$ face of an bcc crystal is extremely open (see Fig. 1.12), missing in-plane nearest neighbour bonds.

The $\{100\}$ bcc surface is similar to the one of fcc crystals, but with an in-plane neighbour distance larger than the nearest neighbour one (unlike for $\{100\}$ fcc). This larger distance enables a 2×2 reconstruction of W(100) as shown in Fig. 1.13. It results in the formation of zig-zag chains.

Semiconductor surfaces of diamond structure crystals

Si and Ge crystallize in diamond structure, an fcc structure with a two atom basis $(0,0,0) a$ and $(\frac{1}{4}, \frac{1}{4}, \frac{1}{4}) a$, a being the lattice constant. The $\underline{III} - \underline{V}$ and many $\underline{II} - \underline{VI}$ compounds crystallize in diamond structure with the two species populating the two positions in the basis. Then the structure is named zinc blende structure.

Fig. 1.14 displays the truncated bulk structures of the diamond lattice. Nearly all semiconductor surfaces reconstruct. The reasoning is as follows:

For the covalently bonded semiconductors it is not possible to redistribute charge from the broken bonds to the remaining bonds, thereby reducing the energy cost associated with them (charge redistribution is easy for metals due to their largely undirectional bonding). Thus the truncated bulk surfaces of semiconductors display highly reactive dangling bonds. In order to reduce surface energy the surface rearranges under the constraint of directional bonding, i.e., by causing only moderate deviations from the preferred bond directions and distances.

Si (111) 7×7

The most famous surface reconstruction which has also been the most influential one in the history of surface science is the (7×7) reconstruction of Si(III). It has been a puzzle for 26 years, from 1959 to 1985. The structure could not be solved with LEED alone. Finally Takayanagi et al. proposed the proper model on the basis of transmission electron microscopy data in 1985. However, without the confirmation by STM the problem would not have been considered to be finally solved.

Up to 880°C the 7×7 is the stable surface phase. It reduces the number of dangling bonds per 7×7 unit cell from 49 to 19 for the prize of elastic energy associated with bond angle distortion. The reconstruction model is called DAS model, as the key structural elements are _dimer_ formation, _adatoms_ and a _stacking fault_. The structure is shown in Fig. 1.15, the stacking fault is best visible in Fig. 1.16 while the STM topograph of Fig. 1.17 highlights the unoccupied states located at the adatoms.

Si (100) 2×1 resp. Si 100 c(4×2)

The truncated bulk structure of Si(100) has two dangling bonds per surface atom. Dimerization costs only moderate elastic energy and lowers the number of dangling bonds by a factor of two.

The dimerization may be described as a σ-band formation, while the remaining e^- of the two db's form a weak π-bond, with the e^- localized. The resulting 2×1 reconstruction shown in Fig. 1.18 is well visible in STM topographs as shown in Fig. 1.19. The two bias inset of Fig. 1.19 shows clearly the localisation of the unoccupied states at the two dimer atoms, while the occupied states have their highest density in between the dimer atoms. This is not the entire truth. As the two e^- of the db's only weakly interact, bonding π and antibonding π^* bands overlap at the Fermi edge. By introducing a symmetry break the system develops a true band gap, leading to a lowering of the π-band and an increase in energy of the π^* band. This is similar to a Jahn-Teller effect. The symmetry break causes a dimer buckling, involving the transfer of an e^- to the higher atom. While the dimers are buckled also at room temperature, the rapid flip-flop motion of the dimer buckling makes the buckling invisible to STM. Only at defects the buckling is frozen. At low temperatures the flip-flop motion is frozen out and a regular arrangement of the buckled dimers in the form of a $c(4 \times 2)$ reconstruction is visible. Fig. 1.20 displays the reconstruction, Fig. 1.21 gives a sketch of the involved electron energetics. Fig. 1.22 displays a summary of the literature and an overview on the historical evolution of the scientific opinions related to the nature of the reconstruction. Note as an interesting detail that the leading theoretical opinion changes after the corresponding experimental discoveries.

Surfaces of ionic crystals

A special stability problem arises for certain surfaces of ionic crystals. Let us consider the ionic crystal to be composed of charged